Modeling Finite-Radius VHF and HF Wire-Antennas for Numerical Dosimetry Applications in Near-Field Interaction Scenarios

Abdelrahman Ijjeh, Marylène Cueille, Jean-Lou Dubard, Michel Ney

Modeling Finite-Radius VHF and HF Wire-Antennas for Numerical Dosimetry Applications in Near-Field Interaction Scenarios

Abdelrahman Ijjeh[1], Marylene Cueille[1], Jean-Lou Dubard[1], Michel Ney[2]
(1) Université Côte d'Azur, CNRS, LEAT, 06903 Sophia Antipolis, France, Jean-Lou.dubard@univ-cotedazur.fr
(2) IMT-Atlantique, Lab-STICC, CS 83818, 29238 Brest Cedex 3, France, michel.ney@imt-atlantique.fr

***Abstract*—This article presents a study of the impact of finite-radius wire antennas in the High Frequency (HF) and the Very High Frequency (VHF) bands on human operators located in the near-field zone. Modeling a finite-radius wire antenna can be a very tricky task, since the antenna parameters, such as the input impedance and the radiated power depend on the wire's shape and the air-gap, as well as its length and the input power source. However, to accurately model the wire shape and the air-gap a very fine resolution is normally needed since they are normally very small in size. In a nutshell, this article studies the impact of the previously mentioned antenna parameters on the Specific Absorbed Rate (SAR) distribution in humans and some possible techniques to speed up the simulation process.**

***Index Terms*— *HF and VHF* antennas, finit-radius wire-antennas computational electromagnetics, numerical dosimetry, near-field interactions, Transmission-Line Matrix (TLM) method, Method of Moments (MoM).**

I. INTRODUCTION

Dosimetry, is defined as the evaluation of absorbed electromagnetic power in living beings exposed to an electromagnetic (EM) field [1]. In several scenarios, practical measurements are very difficult to conduct, due to technological, safety and/or ethical reasons. Creating physical phantoms with EM properties equivalent to those of humans can also be very complex if not impossible for several frequency bands [2]. Therefore, numerical dosimetry via simulation techniques remains the only option for such scenarios. For frequencies under 10 GHz [1], volumic techniques should be used to correctly model the human tissues properties and its internal anatomy. The main and mostly used volumic techniques include the Finite-Difference Time-Domain (FDTD) [3], Finite Elements Method (FEM) [4], Transmission-Line Matrix method (TLM) [5] and the Finite-Integration Technique (FIT) [6]. However, it has been found that the TLM method has several advantages over other techniques for scenarios including very heterogeneous structures such as the human body [7] [8]. That is because, the fields-media interactions happen at the centers of the TLM nodes. On the other hand, in other techniques such as FDTD and FIT empirical rules of averaging are used at the interfaces between different media. Thus, fine resolution is needed to minimize the error introduced by this averaging scheme [8]. Moreover, the TLM method possesses a very efficient and accurate sub-gridding algorithm for arbitrary sub-gridding ratios [9]. This makes the TLM a good candidate for treating multiscale scenarios, such as EM devices including fine details. For wire antennas these fine details can be the wire-cross section, and the feeding air-gap region [10]. Moreover, the time-domain aspect of the TLM allows for wide-band characterization of the antenna system as well as the SAR distributions over the frequency range of interest [11][12].

In [10] it was verified that the input-impedance of the wire-antenna is greatly affected by its cross-section shape/size and the size of the air-gap, for finite-radius as well as for thin-wire antennas. And for a given wire-antenna, say, with a circular cross-section, one has to discretize the cross-section by at least 20 cells to obtain accurate results using the Method of Moments (MoM) [13]. One should keep in mind that MoM method is very efficient for wire-antenna simulations in simple environments (such as in free-space) [14]. However, it becomes extremely costly (in terms of computational resources) when more complex and heterogeneous structures such as the human model are present in the computational domain [15].

Conducting numerical dosimetry simulations for humans in the proximity of propagating devices at the VHF (30MHz-300MHz), the HF (3MHz-30 MHz) [16] or even for frequencies below that can be a very difficult task and should be done carefully. First, the presence of the human in the near-zone of the antenna can impact the antenna propagating conditions, radiation pattern, active-fields/reactive-fields distributions, input impedance…etc. [17] [18]. Therefore, both the human model and the antenna and other nearby elements should be included in the same computational domain. Secondly, as we go down in frequencies, the antenna length increases (to maintain an acceptable level or radiation efficiency). Thirdly, a relatively fine mesh size (for instance 5 mm) is necessary to represent the human model's geometry and its different tissues, to accurately compute the SAR levels in these tissues/organs. Even more, as mentioned above, a very fine resolution is necessary to model the antenna cross-section and the feeding point to accurately evaluate the input impedance and the radiated power. Note that when using existing-thin wire models [19]-[22], one cannot control the real-size of the air-gap, and they are not suitable for finite-radius wire antennas. Finally, as one goes down in frequencies, the time-period of the excitation signal increases. Therefore, a huge number of iterations is necessary to reach the steady-state. That is because for stability reasons, the maximum time-step one can use is controlled by the minimum

Courant–Friedrichs–Lewy (CFL) limit inside the entire computational domain [23].

In this paper, we present a numerical procedure for dosimetry simulations in scenarios involving human subjects in the proximity of HF and VHF antennas. Then, we study the impact of the antenna's cross-section and its input impedance on the computed SAR levels, as well as the impact of the human presence on the antenna's operating conditions.

II. COMPUTATIONAL MODEL

A. Computational Domain Components

As shown in fig. 1 below, the Duke voxel model [24] is exposed to the EM-waves propagated from the wire-antenna in front of it. The antenna is vertically polarized in the midsagittal plane of Duke, and at 20 cm from the chest. Its center is at the same horizontal level of Duke vertical center. For the VHF band antennas, we can use quasi half-wavelength dipoles to obtain maximum efficiency. However, for the HF band or smaller frequencies, electrically smaller antennas are used due to the long wavelengths at such low frequencies.

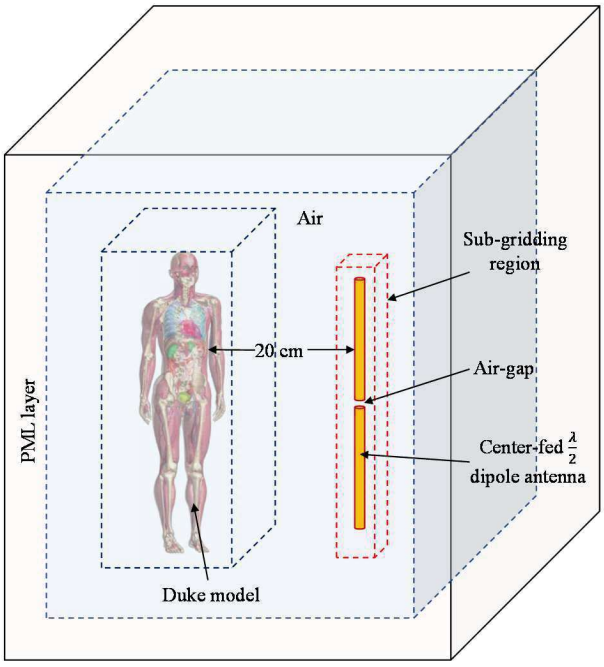

Fig. 1. Duke model in air illuminated by a half-wavelength dipole antenna, sub-gridding is used to enhance the antenna geometrical resolution.

EM media properties of Duke model for different tissues are represented by the following expression [24]:

$$\varepsilon(\omega) = \varepsilon_\infty + \sum_{i=1}^{4} \frac{\Delta\varepsilon_i}{(1+j\omega\tau_i)^{(1-\alpha_i)}} + \frac{\sigma}{j\omega\varepsilon_o} \qquad (1)$$

where ε_∞ is the permittivity at very high frequencies, ε_o is the permittivity of free-space, σ the electric conductivity, τ_i, $\alpha_i$and $\Delta\varepsilon_i$ are different parameters used to adjust the curve fitting model (1) to real measurements [24].

The antenna shown in fig. 1 and fig. 2a, is center-fed by a voltage source using the lumped elements model [25].

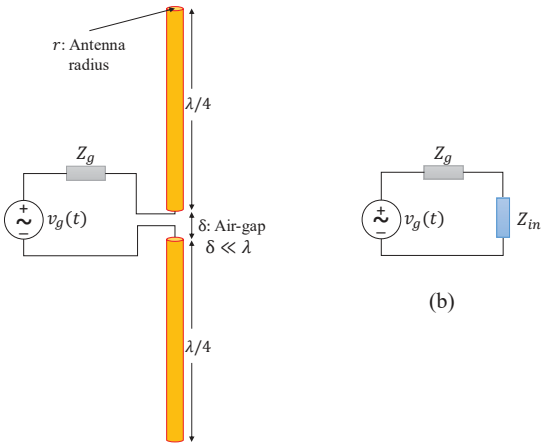

Fig. 2. (a) The wire-antenna used in fig. 1 with its source, (b) Thevenin equivalent circuit of the radiating antenna system.

During the simulation, one knows exactly the temporal profile of the imposed input voltage signal (fig.2a and fig.2b), and the current leaving the source is computed and recorded at every iteration. This permits us to compute the antenna's input impedance Z_{in} [26]. Thus, one can compute the radiated power from the antenna (assuming it is made from a very good conductor, the losses can be neglected). In a numerical simulation, one can chose the generator's internal impedance Z_g to be zero. Therefore, the active radiated power at any given frequency f is defined as [26]:

$$P_r(f) = \frac{1}{2}\mathcal{R}\left(\frac{V_g^2(f)}{Z_{in}^*(f)}\right) \qquad (2)$$

where $\mathcal{R}$ is the real part operator, and $*$ is the conjugate complex.

B. Simulation Technique and Meshing Scheme

As discussed in the introduction, the TLM time-domain method [11] [12] [23] will be used to model the computational domain shown in fig.1. Cartesian sub-gridding (block meshing) will be used around the antenna (the red dashed box in fig. 1). The sub-gridding ratio N_s will be gradually increased to enhance the antenna's geometrical resolution to be as close as possible to the real finite-radius cylindrical shape as shown in fig.3.

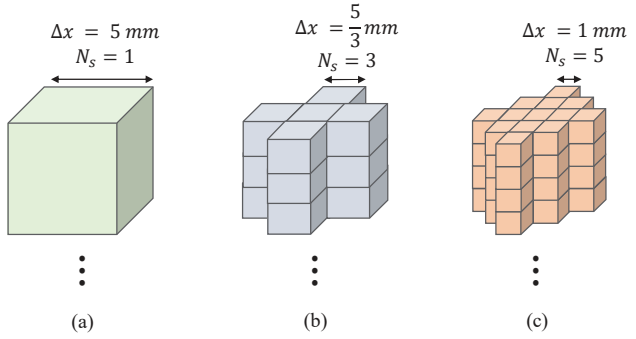

Fig. 3. Different antenna discretization levels, as the sub-gridding ratio N_s increases becomes closer to the cylindrical shape.

C. SAR Normalisation and Comparison Method

Recall that the input impedance of the wire antenna greatly depends on its cross-section shape and dimensions, and the size of the air-gap [10].

The main contribution of this article is to show that even with a relatively coarse meshing of the antenna (corresponding to much less CPU-time), one can obtain accurate SAR levels similar to the case when using a very fine meshing to describe the antenna. The idea is to normalize with respect to the radiated power. Therefore, instead of considering the local SAR values for a given voltage excitation of the antenna, one should normalize with respect to the radiated power from the VHF or HF antenna. That is to normalize the SAR levels to 1 watt of radiated power from the antenna for instance (they can be renormalized to the actual radiated power to eventually obtain correct results that match measurements).

To define a metric for comparing the accuracy of the computed SAR for different antenna discretization schemes shown in fig.3 we are going to use the average relative difference squared. This relative difference is computed as the difference between the SAR distribution obtained in all the phantom's cells for a given N_s sub-gridding ratio of the antenna (we will call it SAR_{Ns}) with respect to the reference SAR_{ref} (corresponding to the case when the antenna is represented with the finest mesh, for instance fig.3c since it is closer to the real cylindrical shape. The relative difference is defined as:

$$R_d(N_s) = \frac{1}{N_D}\sum_{all\ Duke\ cells}\left(\frac{SAR_{ref}-SAR_{Ns}}{SAR_{ref}}\right)^2 \qquad (4)$$

where N_D is the number of cells in Duke model.

III. Results and Discussions

In this section, we present three simulation experiments for the scenario shown in fig.1. Firstly, we illuminate the model by a 300 MHz VHF half-wavelength dipole antenna. In the second experiment the VHF half-wavelength dipole will operate at 100 MHz. In the final experiment the antenna will operate at 20 MHz in the HF band, however, it will be $\lambda/10$-dipole antenna to reduce the computational domain size. In all experiments, the antenna is made of copper of conductivity $\sigma = 5.96 \times 10^7$ (S/m), with a radius equals to 2.5 mm. A 5 mm Duke model resolution was used in all experiments, and a PML layer of 10 cells thickness was used. Global time-step Δt was used in all experiments of 8.33 ps, 2.776 ps and 1.66 ps corresponding to sub-gridding ratios N_s of 1, 3 and 5 respectively. All simulations are conducted using a Fortran TLM solver [27] and were run on a parallel machine.

A. Half-Wave Length Dipole at 300 MHz

In this experiment the Duke model was excited by a half-wavelength dipole antenna of 50 cm length (fig. 1). The input voltage signal is modulated gaussian-pulse with the parameters $(f_0 = 300\ \text{MHz}, sig = 2.77\ \text{ns}, t_0 = 8.32\ \text{ns})$. Three different sub-gridding ratios were used to model the antenna (as shown in fig. 3).

Fig. 4 show the resulting SAR distributions in all three cases after normalizing to 1 radiated watt at 300 MHz.

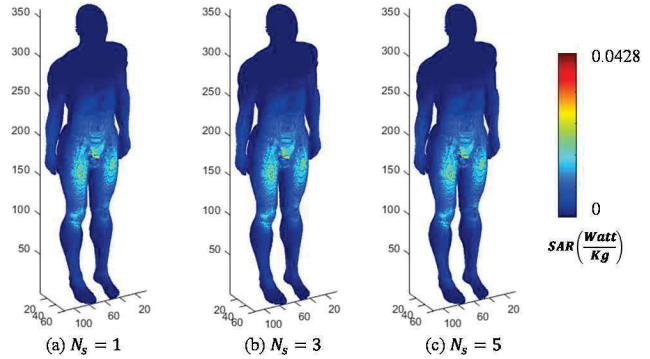

Fig. 4, SAR distributions in Duke model at 300 MHz for different antenna discretization levels as shown in fig. 3.

Considering the case of Ns=5 to be our reference, then $R_d(1) = 4.0967 \times 10^{-4}$ and $R_d(3) = 4.3258 \times 10^{-5}$. Both relative differences are very small. Maximum SAR value for the cases in fig.4 was 0.0428 (W/Kg), it was similar (to the first 4 significant digits) for the three N_s values.

Table I below shows the used computational resources as well as the input impedance of the dipole at 300 MHz. One can notice that the input impedance is very sensitive to the used mesh size in the antenna region (fig. 3). Moreover, one can observe that a crude approximation of the circular antenna cross-section by one cell is enough to obtain the correct SAR values, with significantly less simulation time.

TABLE I. SIMULATION TIME, ANTENNA INPUT INTPUT IMPEDANCE AT 300 MHZ, NUMBER OF PRECESSORS AND NUMBER OF TLM CELLS

N_s	N_{it}	T_{CPU}	Z_{in} (300 MHz)	N_p	N_{cells}
1	8333	31 min	163.1+147.1 Ω	71	9477648
3	25000	1h 29 min	135.3+96.5 Ω	71	9506808
5	40000	2h 25 min	129.2+78.3 Ω	71	9612648

B. Half-Wave Length Dipole at 100 MHz

In this experiment the Duke model was excited by a half-wavelength dipole antenna of 150 cm in physical length (fig. 1). The input voltage signal is modulated gaussian-pulse with the parameters $(f_0 = 100\ \text{MHz}, sig = 8.33\ \text{ns}, t_0 = 41.65\ \text{ns})$. Three different sub-gridding ratios were used to model the antenna (as shown in fig. 3).

Similarly, fig. 5 shows the SAR distributions in the three cases after normalizing to 1 radiated watt at 100 MHz. It is interesting to observe that the SAR levels at 100 MHz are higher than the case of 300 MHz. The reason, is that the antenna length (1.5m) at 100 MHz is closer to the Duke model height (1.77 m) which creates a resonance phenomenon that amplifies the fields and the absorbed energy inside Duke.

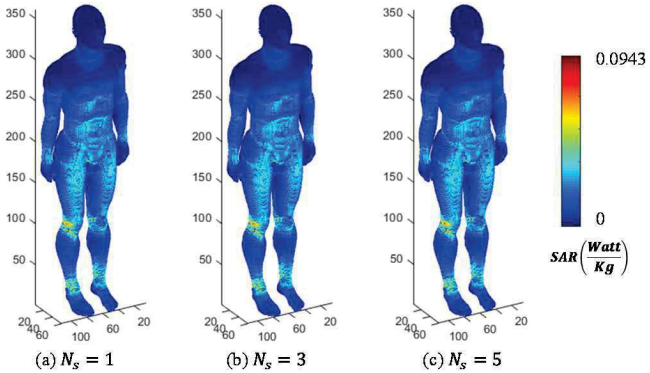

Fig. 5. SAR distributions in Duke model at 100 MHz for different antenna discretization levels as shown in fig. 3.

Similarly, for the case of 100 MHz half-wavelength dipole, we consider the case of $N_s = 5$ to be our reference, then $R_d(1) = 3.7454 \times 10^{-4}$ and $R_d(3) = 1.0279 \times 10^{-4}$. Again, both relative differences are very small.

Table II below shows the used computational resources as well as the input impedance of the dipole at 100 MHz. One can notice that this input impedance is very sensitive to the used mesh size in the antenna region (fig. 3). Moreover, one can observe that a crude approximation of the circular antenna cross-section by one cell is sufficient to obtain the correct SAR values, with a significantly less simulation time. Maximum SAR value for the cases in fig.5 were 0.0943 (W/Kg), 0.0941 (W/Kg) and 0.0928 (W/Kg) for the cases corresponding to fig.5a, fig.5b and fig.5c, respectively. The reason behind these small differences can be explained by the error in Z_{in} (100 MHz) computation. With more iterations one can obtain a more accurate estimation of this input impedance especially for the case of $N_s = 3$ and $N_s = 5$.

TABLE II. SIMULATION TIME, ANTENNA INPUT INTPUT IMPEDANCE AT 100 MHZ, NUMBER OF PRECESSORS AND NUMBER OF TLM CELLS

Ns	N_{it}	T_{CPU}	Z_{in} (100 MHz)	Np	N_{cells}
1	50000	2h 39 min	66.9+j158.8 Ω	71	9477648
3	150000	6h 09 min	59.6+j111.5 Ω	73	9555408
5	250000	10h 54 min	59.0+j93.8 Ω	63	9837648

C. $\lambda/10$- *Length Dipole at 20 MHz*

In this experiment the Duke model was excited by a half-wavelength dipole antenna of 150 cm in physical length (fig. 1). The input voltage signal is modulated gaussian-pulse with the parameters ($f_0 = 60$ MHz, $sig = 10.83$ ns, $t_0 = 75$ ns).). Three different sub-gridding ratios were used to model the antenna (as shown in fig. 3).
Similarly, fig. 5 shows the SAR distributions in the three cases after normalizing to 1 radiated watt at 20 MHz.

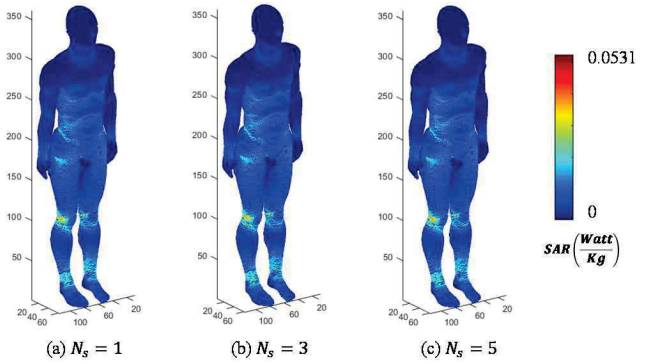

Fig. 6. SAR distributions in Duke model at 20 MHz for different antenna discretization levels as shown in fig. 3.

Similarly, for the case of 20 MHz we consider the case of $N_s = 5$ to be our reference, then $R_d(1) = 0.4541 \times 10^{-4}$ and $R_d(3) = 0.3154 \times 10^{-4}$. Again, both relative differences are very small.

Table III below shows the used computational resources as well as the input impedance of the dipole at 20 MHz. One can notice that this input impedance is very sensitive to the used mesh size in the antenna region (fig. 3). Moreover, one can observe that a crude approximation of the circular antenna cross-section by one cell is sufficient to obtain the correct SAR values, with a significantly less simulation time. Maximum SAR value for the cases in fig.5 were 0.0531 (W/Kg), 0.0531 (W/Kg) and 0.0531 (W/Kg) for the cases corresponding to fig.6a, fig.6b and fig.6c, respectively.

TABLE III. SIMULATION TIME, ANTENNA INPUT INTPUT IMPEDANCE AT 20 MHZ, NUMBER OF PRECESSORS AND NUMBER OF TLM CELLS

Ns	N_{it}	T_{CPU}	Z_{in} (20 MHz)	Np	N_{cells}
1	60000	3h 11 min	21.2-j243.6 Ω	71	9477648
3	180000	9h 33 min	19.6-j235.1 Ω	71	9555408
5	300000	15h 54 min	18.7-j231.7 Ω	71	9837648

IV. CONCLUSION

In this paper we investigated the impact of finite-radius wire antennas in the High Frequency (HF) and the Very High Frequency (VHF) bands on human beings in the near-field zone of the antenna. From the obtained simulation results, one can conclude that a rough approximation of the antenna cross-section (even though it can greatly impact its input impedance and radiated power) is enough to obtain the correct SAR distribution in the body, by normalizing the obtained results with respect to the radiated power. This technique can greatly speed up the numerical dosimetry simulations for scenarios that include human subjects in proximity of wire antennas.

ACKNOWLEDGMENT

This work benefited from access to CINES computing resources through the 2020-A0080505122 resource allocation attributed by GENCI.

REFERENCES

[1] International Commission on Non-Ionizing Radiation Protection (2020). Guidelines on limiting exposure to electromagnetic fields (100 kHz to 300 GHz)". Health Physics 118:483–524.

[2] A. R. Guraliuc et al, "Near-Field User Exposure in Forthcoming 5G Scenarios in the 60 GHz Band," in IEEE Transactions on Antennas and Propagation, vol. 65, no. 12, pp. 6606-6615, Dec. 2017.
W. Chew, et al. Fast and efficient algorithms in computational electromagnetics. Artech House, Inc., 2001.

[3] A. D. Tinniswood, C. M. Furse and O. P. Gandhi, "Computations of SAR distributions for two anatomically based models of the human head using CAD files of commercial telephones and the parallelized FDTD code," in IEEE Transactions on Antennas and Propagation, vol. 46, no. 6, pp. 829-833, June 1998, doi: 10.1109/8.686769.

[4] A. Citkaya and S. Seker. "FEM modeling of SAR distribution and temperature increase in human brain from RF exposure." International Journal of Communication Systems 25.11 (2012): 1450-1464.

[5] A. Ijjeh, et al. "Dosimetry and hyperthermia computation in human tissues in presence of EM-waves using TLM method." 2017 11th European Conference on Antennas and Propagation (EUCAP). IEEE, 2017.

[6] E. Gjonaj, M. Bartsch, M. Clemens, S. Schupp and T. Weiland, "High-resolution human anatomy models for advanced electromagnetic field computations," in IEEE Transactions on Magnetics, vol. 38, no. 2, pp. 357-360, March 2002, doi: 10.1109/20.996096.

[7] Laisné, Alexandre, and Julien Drouet. "Comparison of finite integration technique (fit) and transmission line matrix (tlm) for numerical dosimetry in hf/vhf band." Electromagnetic Compatibility (EMC EUROPE), 2013 International Symposium on. IEEE, 2013.

[8] A. Ijjeh, M. M. Ney, and F. Andriulli. "Behavior of Time-Domain volumic methods in presence of high-contrast media or irregular structured mesh interfaces." 2015 9th European Conference on Antennas and Propagation (EuCAP). IEEE, 2015.

[9] Wlodarczyk, J. "New multigrid interface for the TLM method." Electronics Letters 32.12 (1996): 1111-1112.

[10] M. Ney, et al. "Block Meshing TLM Based Approach for Low Frequency Antennas Characterization." 2019 International Conference on Electromagnetics in Advanced Applications (ICEAA). IEEE, 2019.

[11] Johns, Peter B. "A symmetrical condensed node for the TLM method." IEEE Transactions on Microwave Theory Techniques 35 (1987): 370-377.

[12] A. Farhat et al. "TLM Extension to Electromagnetic Field Analysis of Anisotropic and Dispersive Media: A Unified Field Equation." IEEE transactions on microwave theory and techniques 60.8 (2012):2339-2351.

[13] https://altairhyperworks.com/product/FEKO

[14] D. H. Werner, "A method of moments approach for the efficient and accurate modeling of moderately thick cylindrical wire antennas," in IEEE Transactions on Antennas and Propagation, vol. 46, no. 3, pp. 373-382, March 1998, doi: 10.1109/8.662656.

[15] Antenor de Carvalho, Sérgio, and Leonardo de Souza Mendes. "Scattering of EM waves by inhomogeneous dielectrics with the use of the method of moments and 3-D solenoidal basis functions." Microwave and Optical Technology Letters 23.1 (1999): 42-46.

[16] S. Seybold. Introduction to RF Propagation. John Wiley and Sons. pp. 9–10, 2005.

[17] P. Soontornpipit, C. M. Furse and You Chung Chung, "Design of implantable microstrip antenna for communication with medical implants," in IEEE Transactions on Microwave Theory and Techniques, vol. 52, no. 8, pp. 1944-1951, Aug. 2004, doi: 10.1109/TMTT.2004.831976.

[18] A. Ijjeh, et al. "Numerical dosimetry in human model for 5G and beyond." Union Radio-Scientifique Internationale (URSI-FRANCE 2020 WORKSHOP). 2020.

[19] G. Verissimo, et al. "TLM modeling of thin wires in dispersive media." CEM'11 Computational Electromagnetics International Workshop. IEEE, 2011.

[20] R. Holland and L. Simpson, "Finite-Difference Analysis of EMP Coupling to Thin Struts and Wires," IEEE Trans. Electromagnetic Comp., vol. 23, pp. 88–97, May 1981.

[21] D. Saintier, et al. "An arbitrary oriented thin wire TLM model with optimized interaction domain." 2017 IEEE Radio and Antenna Days of the Indian Ocean (RADIO). IEEE, 2017.

[22] C. Guiffaut, et al. "New oblique thin wire formalism in the FDTD method with multiwire junctions." IEEE Transactions on Antennas and Propagation 60.3 (2012): 1458-1466.

[23] C. Christopoulos, The Transmission-Line Modeling (TLM) Method in Electromagnetics of Synthesis Lectures on Computational Electromagnetics, San Mateo, CA, USA:Morgan Kaufmann, pp. 65-121, 2006.

[24] https://itis.swiss/virtual-population.

[25] A. Balanis. Antenna theory: analysis and design. John wiley & sons, pp. 73-84, 1997.

[26] A. Ijjeh, J-L. Dubard, M. Cueille, O. Makhlouf, M. Ney and A. Laisné.. Solveur TLM multi-physique pour applications en dosimétrie. 6ième Journées d'études " Electromagnetisme et guerre Electronique", Nov 2017, Toulouse, France.

[27] P. Russer, B. Isele, M. Sobhy and E. A. Hosny, "A general interface between TLM models and lumped element circuit models," 1994 IEEE MTT-S International Microwave Symposium Digest (Cat. No.94CH3389-4), San Diego, CA, USA, 1994, pp. 891-894 vol.2, doi: 10.1109/MWSYM.1994.335214.